Electronic structure and transport anisotropy of Bi_2Te_3 and Sb_2Te_3

B. Yu. Yavorsky,[1,*] N. F. Hinsche,[1] I. Mertig,[1,2] and P. Zahn[1]

[1] *Institut für Physik, Martin-Luther-Universität Halle-Wittenberg, D-06099 Halle, Germany*

[2] *Max-Planck-Institut für Mikrostrukturphysik, Weinberg 2, D-06120 Halle, Germany*

(Dated: December 25, 2021)

Abstract

On the basis of detailed *ab initio* studies the influence of strain on the anisotropy of the transport distribution of the thermoelectrics Bi_2Te_3 and Sb_2Te_3 was investigated. Both tellurides were studied in their own, as well as in their co-partners lattice structure to gain insight to the electrical transport in epitaxial heterostructures composed of both materials. It is shown, that the anisotropy of the transport distribution overestimates the experimental findings for Bi_2Te_3, implying anisotropic scattering effects. An increase of the in-plane lattice constant leads to an enhancement of the transport anisotropy for p-doping, whereas the opposite occurs for n-doping. The recent findings and special features of the transport distribution are discussed in detail in relation to the topology of the band structures.

PACS numbers: 71.15.Mb, 71.15.Rf, 71.20.Nr, 72.20.Pa

Keywords: thermoelectric materials, *ab initio* band structure, Boltzmann formalism, transport distribution, effective mass approximation

I. INTRODUCTION

Thermoelectric (TE) materials have huge potential for power generation, heat pumping, and refrigeration. However, their practical application is restricted because of the low performance of the TE devices compared to traditional fossil fuel power generators and compressor-based refrigerators[2]. A high performance TE material has to be a good electrical conductor as well as a poor thermal conductor and, at the same time, possess a large Seebeck coefficient[3]. Quantitatively the efficiency of TE devices is expressed by the dimensionless figure of merit ZT,

$$ZT = \alpha^2 \sigma T/(\kappa_L + \kappa_e), \tag{1}$$

where α, σ, T are the Seebeck coefficient, electrical conductivity and absolute temperature, and κ_L, κ_e are phonon and electron contributions to the total thermal conductivity, respectively.

Bismuth and antimony tellurides, Bi_2Te_3, Sb_2Te_3, and the alloys based on these materials play a significant role for thermoelectric technology. Already early studies of the $(Bi_x,Sb_{2-x})Te_3$ compounds in the late 1950s reported $ZT \sim 1$ at room temperature[4], confirmed by further experiments[5]. This value remains, even to date, the maximal one available at room temperature for bulk materials. Current progress in nanostructure fabrication, in particular, epitaxial growth of high-quality superlattices[6], encourages the possibility of significant performance improvement of TE devices. Venkatasubramanian *et al.* reported $ZT \sim 2.4$ and $ZT \sim 1.45$ at 300K for p-type and n-type Bi_2Te_3/Sb_2Te_3 superlattices, respectively[7].

These experimental advances motivated extensive theoretical studies of the electronic structure of the bulk bismuth and antimony telluride aimed to understand the possible origin of the increased thermoelectic performance in the multilayered structures. While in the previous years only few *ab initio* band-structure calculations of the bulk bismuth telluride[8,9] could be mentioned, in the last decade various aspects of the electronic structure of both pure and doped bulk Bi_2Te_3 and Sb_2Te_3 as well as their transport properties were discussed in Ref.[10–22]. *Ab initio* studies of the electronic structure and the transport properties of Bi_2Te_3/Sb_2Te_3 superlattices were also reported[23].

An explanation of directional anisotropy of the transport properties in Bi_2Te_3/Sb_2Te_3 superlattices could play a crucial role for the understanding of their increased figure of

merit. Venkatasubramanian *et al.*[7] found a strong dependence of the anisotropy of the carrier mobility on both the superlattice period and the relative thickness of the constituents. The enhancement of the electrical conductivity parallel to the epitaxial growth direction, i.e. the trigonal axis of the rhombohedral lattice of bismuth and antimony tellurides, together with the possibility to suppress the lattice thermal conductivity κ_L along this direction could provide the desirable ZT enhancement.

In this study we concentrate on the anisotropy of the transport properties in the bulk Bi_2Te_3 and Sb_2Te_3 as a first step on a way of understanding the corresponding properties of the Bi_2Te_3/Sb_2Te_3 superlattices. Since epitaxial growth always implies lattice distortions we included, as discussed below, the effect of the lattice relaxation in our study.

II. CRYSTAL STRUCTURE

Both bismuth and antimony telluride possess the rhombohedral crystal structure with five atoms, i.e. one formula unit, per unit cell belonging to the space group D_{3d}^5 ($R\bar{3}m$). Experimental lattice parameters[24] are $a_{BiTe}^{rh} = 10.473$Å, $\theta_{BiTe} = 24.17°$, and $a_{SbTe}^{rh} = 10.447$Å, $\theta_{SbTe} = 23.55°$, were θ is the angle between the rhombohedral basis vectors of the length a^{rh}. In order to emphasize the layered character of this structure it is convenient to rearrange it into the hexagonal unit cell built up by three formula units, as shown in Fig.1. The hexagonal cell contains 15 atoms grouped in the 3 'quintuple' layers, Te1-Bi(Sb)-Te2-Bi(Sb)-Te1, where Te1 and Te2 are two different crystal kinds of tellurium atoms. The 'hexagonal' lattice parameters are $a_{BiTe}^{hex} = 4.384$Å, $c_{BiTe}^{hex} = 30.487$Å, and $a_{SbTe}^{hex} = 4.264$Å, $c_{SbTe}^{hex} = 30.458$Å, for Bi_2Te_3 and Sb_2Te_3, respectively. In bismuth telluride the nearest interatomic distances between the individual monolayers inside the 'quintuple' blocks are 3.07Å for Te1-Bi and 3.25Å for Bi-Te2. Two adjacent 'quintuple' layers in Bi_2Te_3 are separated by somewhat longer distance, 3.63Å for Te1-Te1. In the antimony telluride these distances are 2.98Å for Te1-Sb, 3.17Å for Sb-Te2 inside the 'quintuple' blocks, and 3.74Å for Te1-Te1 between the blocks.

In the Bi_2Te_3/Sb_2Te_3 multilayers atoms change their bulk positions due to the mismatch of the lattice parameters. The description of the realistic crystal structure of the multilayers is out of the scope of this study. Nonetheless, we modeled Bi_2Te_3 with the experimental lattice parameters and interatomic distances of Sb_2Te_3, and vice versa. Since both materials

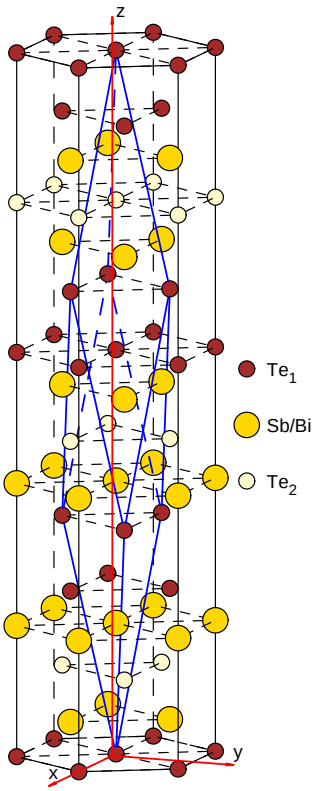

FIG. 1: The rhombohedral unit cell superimposed with the hexagonal one to emphasize the layered character of the material.

have very similar lattice parameter c^{hex} along z-axis this variation is essentially compression and extension of the lattice in (xy) plane for bismuth and antimony telluride, respectively. We assume that one could estimate the effect of the lattice relaxation on the electronic and transport properties in the Bi_2Te_3/Sb_2Te_3 heterostructures from these two limiting cases.

III. CALCULATIONAL DETAILS

Calculations of the electronic structures were performed by means of the screened Korringa-Kohn-Rostoker Green's function method[25] in the atomic sphere approximation (ASA) within the local density approximation of the density functional theory in the parameterization of Vosko *et al.*[26]. It is generally recognized that the effects of spin-orbit coupling are mandatory for the correct treatment of the band structure in these materials. Therefore we used a fully relativistic version of the method based on the Dirac equation[27]. The obtained self-consistent band structures were used for the calculations of the transport

distribution $\sigma_{\alpha\beta}$ within the Boltzmann formalism assuming a constant relaxation time τ[28],

$$\sigma_{\alpha\beta}(E) = \tau \frac{e^2}{(2\pi)^3 \hbar} \sum_j \int\limits_{\varepsilon^j(\mathbf{k})=E} dS \frac{v^j_\alpha(\mathbf{k}) v^j_\beta(\mathbf{k})}{\mid \mathbf{v}^j(\mathbf{k}) \mid}, \qquad \mathbf{v}^j(\mathbf{k}) = \frac{1}{\hbar} \bigtriangledown_{\mathbf{k}} \varepsilon^j(\mathbf{k}), \tag{2}$$

where $\varepsilon^j(\mathbf{k})$ is the j-th band energy at the $\mathbf{k}$-point of the Brillouin zone (BZ), α and β denote cartesian coordinates. We assume the relaxation time to be isotropic. In this approximation the transport anisotropy ratio σ_{xx}/σ_{zz} is independent on the relaxation time, and we do not have to specify it.

The $\mathbf{k}$-space integration over the isoenergetic surfaces was performed with the tetrahedron method on the Blöchl mesh[32] of 96×96×96 points in the whole BZ. In the energy intervals of the width about 0.1 eV in the vicinity of both band edges the integration was refined by means of an adaptive mesh up to 4×4×4 times as dense as the original one. As a convergence criterium we used the values of the transport anisotropy ratio calculated from the effective mass approximation at the band extrema[29].

IV. ELECTRONIC STRUCTURES AND TRANSPORT PROPERTIES

The electronic band structures for Bi_2Te_3 and Sb_2Te_3 for both experimental and strained lattices are shown in Fig.2. The positions of the high-symmetry points in the BZ of the rhombohedral structure are denoted in Fig.3. Our results at the experimental lattice parameters agree well with the previous *ab initio* studies of Mishra *et al.*[9], Larson *et al.*[10] for Bi_2Te_3, and of Eremeev *et al.*[22] both for Bi_2Te_3 and Sb_2Te_3. At the same time the calculations made with the full-potential linearized augmented plane wave method (FLAPW) result in slightly different band structures for the bismuth and antimony tellurides at both the experimental[11–14,20] and strained[19,21] lattices. The key question of the band structure of Bi_2Te_3 and Sb_2Te_3 is the position of the valence band maximum (VBM) and conduction band minimum (CBM) in the BZ. The calculations of Ref.[11–14,20] result in a six-valley both VBM and CBM located in the symmetry plane (ΓZU) in agreement with experiments for both the bismuth[30] and antimony[31] tellurides. Unlike these results, in our case the CBM of Bi_2Te_3, at both lattice parameters, a_{BiTe} and a_{SbTe}, is a two-valley minimum located on the symmetry line ΓZ, similarly to Ref.[9]. For Sb_2Te_3 at the experimental lattice parameters we found a direct band gap located at the center of the BZ, while at the larger in-plane lattice constant both six-valley VBM and CBM lie in the symmetry plane (ΓZU).

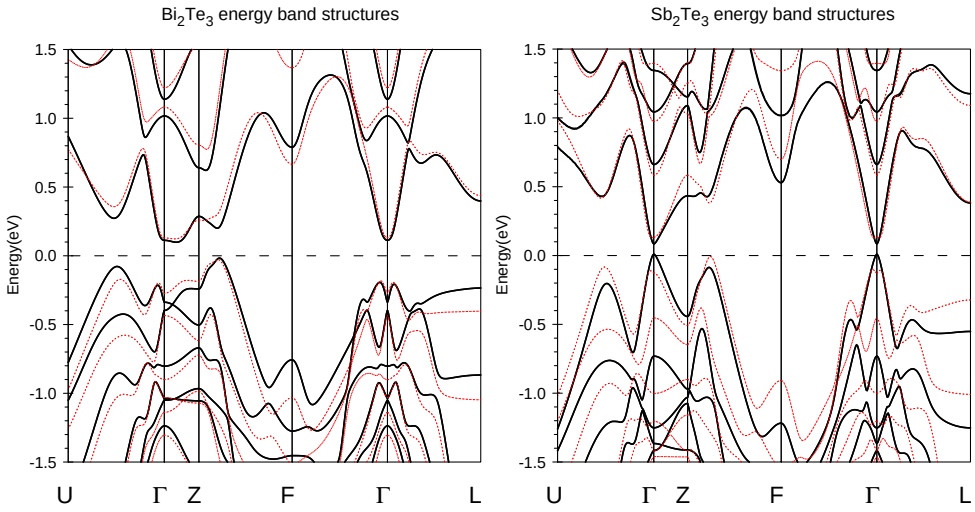

FIG. 2: Band structures of Bi_2Te_3 and Sb_2Te_3 along symmetry lines for both experimental (solid) and strained (dashed) lattices. Energies are given relative to the VBM.

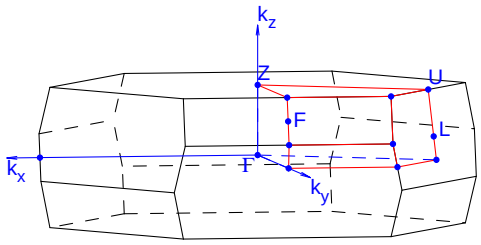

FIG. 3: Brillouin zone of the rhombohedral lattice.

In contrast to our results Thonhauser[15] found that the increase of the lattice parameters in Sb_2Te_3 led to the formation of a direct band gap at the Γ point. On the other hand, the negative hydrostatic pressure discussed in Ref.[15] implies an increase of both in-plane and out-of-plane lattice parameters in comparable degree, while in our study essentially the first one is included. Additionally, calculations in Ref.[15] were performed for optimized atomic positions with respect to the total energy, which can affect the band structure of antimony telluride[19].

As already discussed[9,11], these differences in the band structures are probably due to the non-spherical part of the potential, which is not included in the ASA. At the same time, as discussed below, these differences have no significant impact on the transport distribution $\sigma(E)$. The details of the band structures for all four systems are compiled in Table I.

The calculated transport distribution of Bi_2Te_3 at both the experimental, $a = a_{BiTe}$, and

TABLE I: Band structure parameters: Band gap in eV, positions of VBM and CBM in crystallographic coordinates, effective masses in electron mass units, principal axes $\mathbf{e}_i$ in cartesian coordinates, and transport anisotropy ratio from the effective mass approximation.

Bi_2Te_3				
Lattice parameters	$a = a_{BiTe}$		$a = a_{SbTe}$	
Gap(eV)	0.105		0.129	
Extremum	VBM	CBM	VBM	CBM
Position	0.517 0.366 0.366	0.173 0.173 0.173	0.405 0.405 0.335	0.151 0.151 0.151
Effective masses				
m_1	-0.024	0.178	-0.039	0.154
m_2	-0.134	0.178	-0.077	0.154
m_3	-1.921	0.835	-0.207	1.370
Principal axes				
$\mathbf{e}_1$	0.500 -0.867 0.000	1.000 0.000 0.000	0.866 0.499 -0.024	1.000 0.000 0.000
$\mathbf{e}_2$	0.600 0.346 0.721	0.000 1.000 0.000	0.500 -0.867 0.000	0.000 1.000 0.000
$\mathbf{e}_3$	0.625 0.361 -0.693	0.000 0.000 1.000	0.021 0.012 0.999	0.000 0.000 1.000
σ_{xx}/σ_{zz}	5.452	4.700	4.020	9.013
Sb_2Te_3				
Latt. param.	$a = a_{SbTe}$		$a = a_{BiTe}$	
Gap(eV)	0.090		0.140	
Extremum	VBM	CBM	VBM	CBM
Position	0.000 0.000 0.000	0.000 0.000 0.000	0.547 0.392 0.392	0.004 0.020 0.020
Effective masses				
m_1	-0.054	0.045	-0.039	1.124
m_2	-0.054	0.045	-0.083	1.774
m_3	-0.102	0.114	-2.046	6.861
Principal axes				
$\mathbf{e}_1$	1.000 0.000 0.000	1.000 0.000 0.000	0.500 -0.867 0.000	-0.316 -0.183 0.931
$\mathbf{e}_2$	0.000 1.000 0.000	0.000 1.000 0.000	0.594 0.343 0.727	0.500 -0.867 0.000
$\mathbf{e}_3$	0.000 0.000 1.000	0.000 0.000 1.000	0.630 0.363 -0.686	0.806 0.465 0.365
σ_{xx}/σ_{zz}	1.889	2.507	2.397	2.080

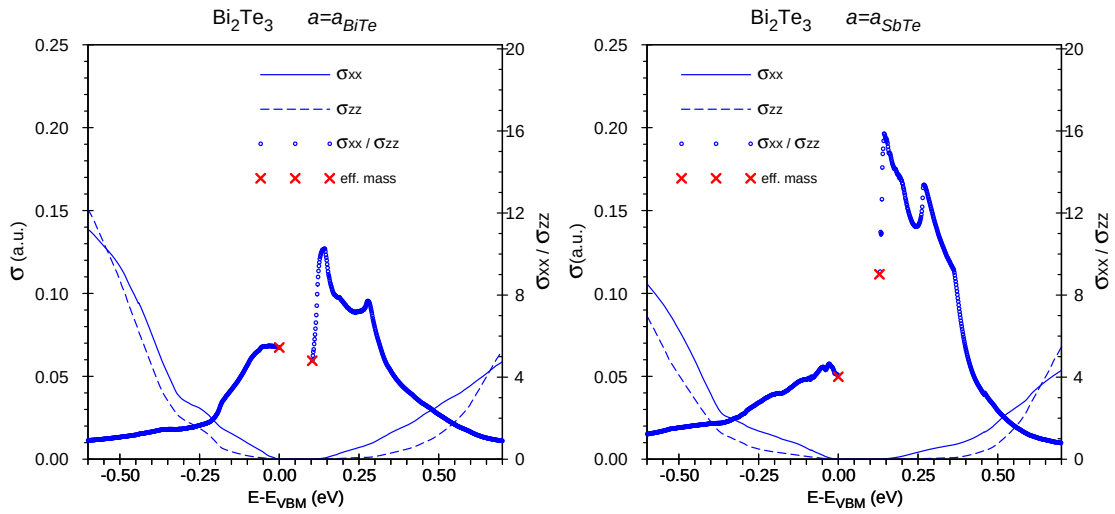

FIG. 4: Transport distribution $\sigma_{xx}(E)$ and $\sigma_{zz}(E)$ and the transport anisotropy σ_{xx}/σ_{zz} for Bi_2Te_3 at the experimental and compressed lattice parameters. Crosses at the band edges mark the σ_{xx}/σ_{zz} ratio derived from the effective mass model[29] using the parameters of Table I.

compressed, $a = a_{SbTe}$, lattice parameters are shown in Fig.4 together with the anisotropy ratio σ_{xx}/σ_{zz}. In terms of the rigid band model the energies below and above the band gap simulate p- and n-doping respectively. While for p-doping close the VBM σ_{xx}/σ_{zz} varies smoothly approaching the limiting value, the ratio increases drastically and forms a prominent two-peak structure for n-doping case. This structure originates from the two topological transformations of the constant energy surfaces in the conduction band. Fig.5(a) shows the contour plot of $\varepsilon(\mathbf{k})$ for Bi_2Te_3 at $a = a_{BiTe}$ in the plane (ΓZU) for energies 0 to 0.19eV relative to the conduction band edge. The main features of the band structure are the global CBM on the line ΓZ, the local conduction band minimum (LCBM) at (0.666,0.602,0.602), and two saddle points s_1 at (0.722 ,0.667, 0.667) and s_2 at (0.493,0.461,0.461), in crystallographic coordinates. The saddle point s_1 occurs at $E - E_{CBM} = 0.04$eV and causes the first peak of σ_{xx}/σ_{zz}, while s_2 appears at 0.17eV and forms the second peak. At room temperature the chemical potential would be located in the saddle point s_1 or s_2, for an electron carrier concentration of about $N = 3.0 \times 10^{19} cm^{-3}$ or $N = 1.5 \times 10^{20} cm^{-3}$, respectively. The location of the LCBM in our band structure calculation is close to the position of the six-valley CBM reported in Ref.[11–14,19,20], and the energy difference between these two minima, $E_{LCBM} - E_{CBM}$=0.04eV, is quite small. At the same time the saddle point s_2 close to the local band maximum at Z was found as well in agreement with these calculations. A

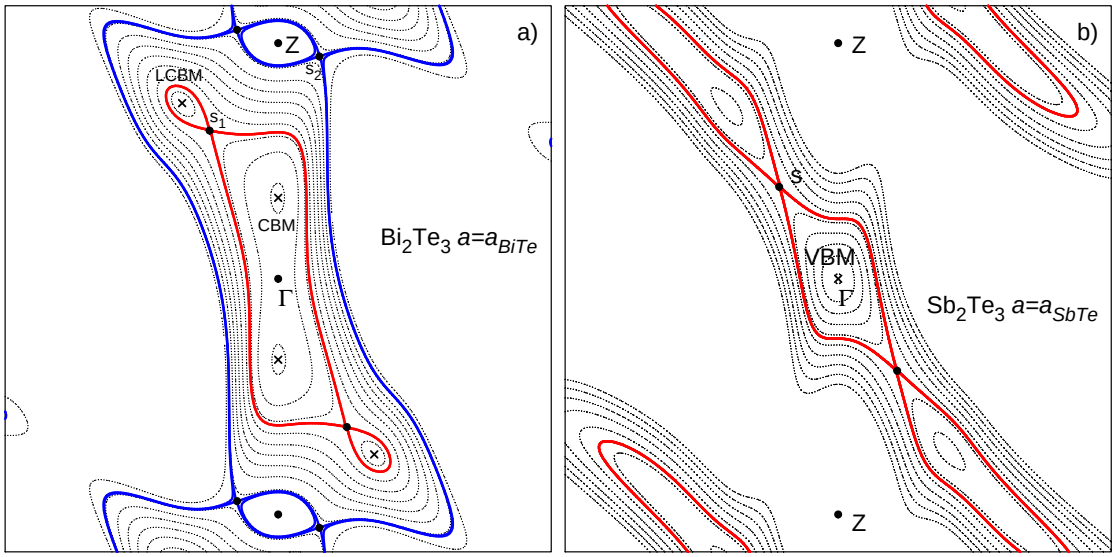

FIG. 5: Contour plots of $\varepsilon(\mathbf{k})$ at the experimental lattice constants in the plane (ΓZU)
(a) Bi_2Te_3, 10 isolines for $(E - E_{CBM})$ at 0 to 0.19eV with a constant increment(dotted), additionally, 2 isolines at $E - E_{CBM} = 0.04$eV and $E - E_{CBM} = 0.17$eV with the saddle points s_1 and s_2, respectively (bold), the positions of the CBM and the LCBM are marked with crosses.
(b) Sb_2Te_3, 10 isolines for $(E - E_{VBM})$ at -0.24 eV to 0 with a constant increment (dotted), additionally, 1 isoline with the saddle point s (bold), the position of the VBM is marked with a cross.

slight shift of the energies at the CBM and the LCBM would bring these two band structures in accordance. Since the saddle point s_1 lies close to the line connecting the CBM and the LCBM this modification would not affect remarkably the band structure topology. Moreover, the transport anisotropy σ_{xx}/σ_{zz} at the LCBM from the effective mass approximation is 4.95, which is fairly close to 4.7 at the CBM. This indicates that the transport anisotropy of the bismuth telluride at the experimental lattice parameters is stable with respect to small modifications of the band structures with a two- and six-valley CBM, respectively.

In Bi_2Te_3 the in-plane compression of the lattice parameters from $a = a_{BiTe}$ to $a = a_{SbTe}$ increases the transport anisotropy ratio at the conduction band edge remarkably. Within the effective mass approximation this can be explained by the enhancement of the ratio $m_\perp/m_\parallel$ due to the expansion of the BZ in xy plane. At the same time σ_{xx}/σ_{zz} decreases at the valence band edge. In this case the compression of the lattice results in a re-orientation of the longest axis of the effective mass ellipsoid near the VBM closer to the z axis, which

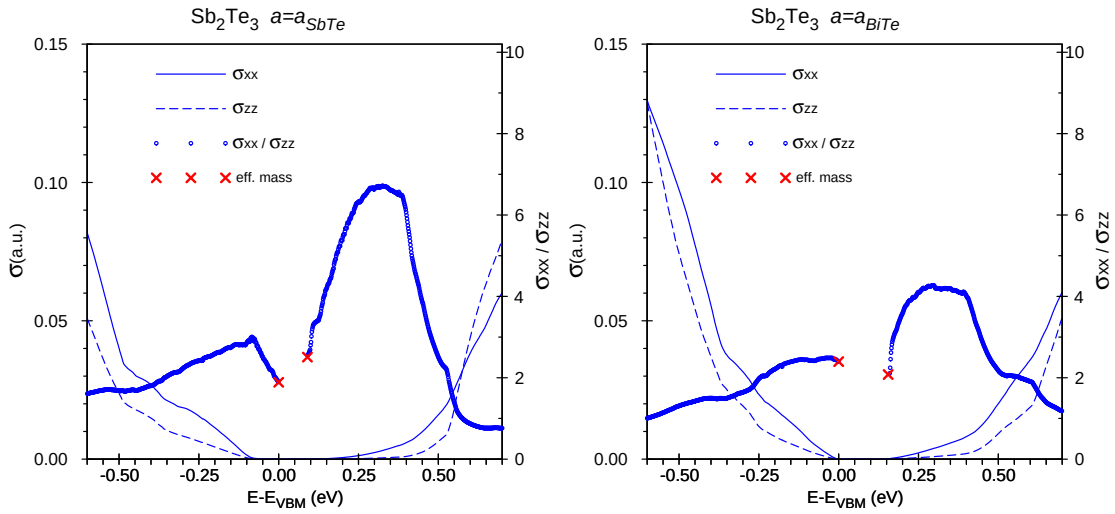

FIG. 6: Transport distribution and the transport anisotropy for Sb_2Te_3 at the experimental and expanded lattice parameters. Crosses at the band edges mark the σ_{xx}/σ_{zz} derived from the effective mass model[29] using the parameters of Table I.

lead to an increase of the transport anisotropy ratio, and at the same time decreases the anisotropy of the dominating effective masses m_2 and m_3 (see Table I). The last effect prevail over the enhancement of σ_{xx}/σ_{zz} due to the rotation of the effective mass ellipsoid. Fig.6 shows the transport distribution and the anisotropy ratio of Sb_2Te_3 at both $a = a_{SbTe}$ and $a = a_{BiTe}$. The kink of the anisotropy ratio at the experimental lattice parameters is induced by the saddle point s =(0.831, 0.784, 0.784) at $E - E_{VBM} = 0.116$ eV, which corresponds to a hole carrier concentration of $N = 5.8 \times 10^{19} cm^{-3}$ at 300K. This topology is illustrated in Fig.5(b), which shows the contour plot of $\varepsilon(\mathbf{k})$ in the valence band of the antimony telluride for energies -0.24 eV to 0 relative to E_{VBM}. The in-plane expansion of the lattice parameter increases the density of the occupied states near the valence band edge and suppresses the kink. The transport anisotropy ratio increases with the in-plane compression of the BZ at the valence band edge, and, at the same time, decreases at the conduction band edge due to the larger angle between the z axis and the largest axis of the effective mass ellipsoid, similarly to the discussed changes in bismuth telluride.

V. CONCLUSIONS

On the basis of *ab initio* electronic structures obtained with the fully relativistic KKR method we studied the anisotropy of the transport properties of the bismuth and antimony tellurides in the constant relaxation time approximation within the Boltzmann formalism. In addition to the systems with the experimental lattice parameters we modeled bismuth telluride within the lattice of Sb_2Te_3, and vice versa. We found that a decrease of the in-plane lattice parameters increases the transport anisotropy for the n-doping and, at the same time, decreases the anisotropy for the p-doped case. This effect can be understood within the effective mass approximation at the valence band maximum and conduction band minimum, respectively.

* Electronic address: bogdan.yavorsky@physik.uni-halle.de

* Corresponding author.

Email address: bogdan.yavorsky@physik.uni-halle.de

[2] F. J. DiSalvo, Science **285**, 703 (1999)

[3] L. E. Bell, Science **321**, 1457 (2008)

[4] C. B. Satterthwaite and R. W. Ure, Phys. Rev. **108**, 1164 (1957),

F. D. Rosi, B. Abeles, and R. S. Jensen, J. Phys. Chem. Solids **10**, 191 (1959)

[5] J. P. Fleurial, L. Gailliard, R. Triboulet, H. Scherrer, and S. Scherrer, J. Phys. Chem. Solids **49**, 1237 (1988),

T. Caillat, M. Carle, P. Pierrat, H. Scherrer, and S. Scherrer, J. Phys. Chem. Solids **53**, 1121 (1992)

[6] R. Venkatasubramanian, T. Colpitts, B. O'Quinn, S. Liu, , N. El-Masry, and M. Lamvik, Appl.Phys.Lett. **75**, 1104 (1999)

[7] R. Venkatasubramanian, E. Siilova, T. Colpitts, and B. O'Quinn, Nature **413**, 597 (2001)

[8] G. A. Thomas, D. H. Rapkine, R. B. Van Dover, L. F. Mettheiss, W. A. Sunder, L. F. Schneemeyer, and J. V. Waszczak, Phys. Rev. B **46**, 1553 (1992)

[9] S. K. Mishra, S. Satpathy, and O. Jepsen, J.Phys.: Condens. Matter **9**, 461 (1997)

[10] P. Larson, S. D. Mahanti, and M. G. Kanatzidis, Phys. Rev. B **61**, 8162 (2000)

[11] S. J. Youn and A. J. Freeman, Phys. Rev. B **63**, 085112 (2001)

[12] T. J. Scheidemantel, C. Ambrosch-Draxl, T. Thonhauser, J. V. Badding, and J. O. Sofo, Phys. Rev. B **68**,125210 (2003)

[13] T. Thonhauser, T. J. Scheidemantel, J. O. Sofo, J. V. Badding, and G. D. Mahan, Phys. Rev. B **68**,085201 (2003)

[14] P. Larson, Phys. Rev. B **68**, 155121 (2003)

[15] T. Thonhauser, Solid State Commun. **129**, 249 (2004)

[16] M. Kim, A. J. Freeman, and C. B. Geller, Phys. Rev. B **72**, 035205 (2005)

[17] P. Larson, Phys. Rev. B **74**, 205113 (2006)

[18] S. Lee, and P. von Allmenn, Appl. Phys. Lett. **88**, 022107 (2006)

[19] G. Wang and T. Cagin, Phys. Rev. B **76**, 075201 (2007)

[20] B.-L. Huang, and M. Kaviany, Phys. Rev. B **77**, 125209 (2008)

[21] M. S. Park, J.-H. Song, J. E. Medvedeva, M. Kim, I. G. Kim, and A. J, Freeman, Phys. Rev. B **81**, 155211 (2010)

[22] S. V. Eremeev, Yu. M. Koroteev, and E. V. Chulkov, JETP Letters **91**, 387 (2010)

[23] H. Li, D. Bilc, and S. D. Mahanti, Mat. Res. Soc. Symp. Proc. **793**, 8.37 (2004)

[24] O. Madelung, M. Schulz, H. Weiss (Eds.) Landolt-Börnstein, New Series, Group III, vol. 17f, (Springer, New York, 1983)

R. W. G. Wyckoff , Crystal Structures 2, J. (Wiley and Sons, New York, 1964)

Th. L. Anderson , H. Krause, H. Brigitte: Acta Crystallogr. B 30, 1307 (1974)

[25] R. Zeller, P. H. Dederichs, B. Újfalussy, L. Szunyogh, and. P. Weinberger, Phys. Rev. B **52**, 8807 (1995)

N. Papanikolau, R. Zeller, and P. H. Dederichs, J. Phys.: Condens. Matter **14**, 2799 (2002)

[26] S. H. Vosko, L. Wilk, and M. Nusair, Can. J. Phys. **58**, 1200 (1980)

[27] M. Gradhand, M. Czerner, D. V. Fedorov, P. Zahn, B. Yu. Yavorsky, L. Szunyogh, and I. Mertig, Phys. Rev. B **80**, 224413 (2009)

[28] J. M. Ziman, *Principles of the Theory of Solids* (Cambridge University Press, Cambridge, 1972).

[29] P. Zahn, N. F. Hinsche, B. Yu. Yavorsky, and I. Mertig, to be published (2011)

[30] J. R. Drabble, R. D. Groves, and R. Wolfe, Proc. Phys. Soc. London **71**, 430 (1958)

R. B. Mallinson, J. A. Rayne, and R. W. Ure, Jr., Phys. Lett **19**, 545 (1965)

[31] H. Schwarz, G. Björck, and O. Beckman , Soli. State Commun. **5**, 905 (1967)

V. A. Kulbachinskii, Z. M. Dashevskii, M. Inoue, M. Sasaki, H. Negishi, W. X. Gao, P. Lostak, J. Horak, and A. de Visser, Phys. Rev. B **52**, 10915 (1995)

[32] P. E. Blöchl, O. Jepsen, and O. K. Andersen, Phys. Rev. B **49**, 16223 (1994)